Low frequency magnetic field monitoring using anisotropic magnetoresistances

I. Mateos[a,b,*], J. Ramos-Castro[a,c], A. Lobo[a,b,1]

[a] *Institut d'Estudis Espacials de Catalunya, 08034 Barcelona, Spain*
[b] *Institut de Ciències de l'Espai (CSIC), 08193 Bellaterra, Spain*
[c] *Departament d'Enginyeria Electrònica, Universitat Politècnica de Catalunya, 08034 Barcelona, Spain*

Abstract

A dedicated study about magnetic sensing techniques based on anisotropic magnetoresistive sensors has revealed to be a suitable technology for low-frequency space applications like the eLISA mission. Low noise magnetic measurements at the sub-millihertz frequencies have been carried out using different noise reduction techniques in the signal conditioning circuit, where conventional techniques reversing the sensor bridge excitation do not reduce the potential $1/f$ noise of the magnetoresistors, and alternative methods are necessary. In addition, a low-frequency noise analysis of the signal conditioning circuits has been performed in order to identify and minimize the different main contributions from the overall noise. The results for chip-scale magnetoresistances exhibit similar noise along the eLISA bandwidth (0.1 mHz − 1 Hz) than the bulky fluxgate magnetometers used in its precursor mission LISA Pathfinder.

Keywords: eLISA, magnetoresistors, low-frequency noise

1. Introduction

eLISA (evolved Laser Interferometer Space Antenna) is a space-based observatory proposed as a large space mission of the European Space Agency (ESA) and conceived to directly detect low-frequency gravitational radiation between 0.1 mHz to 1 Hz. This bandwidth, which is not observable from Earth, is expected to reveal some of the most exciting GW sources, such as massive black holes coalescence, compact binaries, and extreme mass ratio inspirals [1]. eLISA will be make up by three drag-free spacecraft (one "mother" and two "daughters") in equilateral triangle configuration with one-million-kilometer side. Each side forms a two-link interferometer between freely floating test masses (TMs) that act as the geodesic reference mirrors for the gravitational wave measurement. Hence, the changes between the TM distances caused by a GW shift the phase readout of inter-satellite laser interferometer. However, the weakness of GWs distort in a very small manner the geometry of space-time, therefore, measurements of exceedingly small displacements between the two free-falling TMs are necessary for their detection. For this reason, the environment surrounding the TM must be shielded from non-gravitational forces, which can perturb the free-floating motion bodies preventing the GW detection.

The free-fall performance of the TM for eLISA is customarily defined in terms of linear spectral density of acceleration noise. At low frequency (0.1 mHz), the residual acceleration noise induced by the parasitic effects are required to be lower than $3\,\mathrm{fm\,s^{-2}\,Hz^{-1/2}}$ per test mass. Consequently, environmental conditions around the TMs such as thermal, magnetic and random charging fluctuations need to be under stringent control [2]. Among the residual disturbance sources, a significant fraction of the total acceleration budget is due to the magnetic environment created by the interplanetary magnetic field, electronic units, and other components such as the micro-thrusters, batteries, solar panel cells, etc. The non-gravitational force induced by the magnetic field $\mathbf{B}$ and its gradient is caused by the magnetic properties of the TM, i.e., the magnetization $\mathbf{M}$ and susceptibility χ. This spurious force on the TM volume V is given by

$$\mathbf{F} = \left\langle \left[\left(\mathbf{M} + \frac{\chi}{\mu_0} \mathbf{B} \right) \cdot \nabla \right] \mathbf{B}, \right\rangle V \qquad (1)$$

where $\mu_0 = 4\pi \cdot 10^{-7}\,\mathrm{m\,kg\,s^{-2}\,A^{-2}}$, and $\langle \cdots \rangle$ denotes TM volume average of the enclosed quantity. Then, if the second order term are neglected, the force fluctua-

*Corresponding author
Email address: mateos@ice.csic.es (I. Mateos)
[1] Deceased

tions along the x-component axis are estimated by

$$\delta F_x = V\langle \delta\mathbf{M}\cdot\boldsymbol{\nabla} B_x\rangle + V\langle \mathbf{M}\cdot\delta(\boldsymbol{\nabla} B_x)\rangle + \\ + \frac{\chi V}{\mu_0}\langle \delta\mathbf{B}\cdot\boldsymbol{\nabla} B_x\rangle + \frac{\chi V}{\mu_0}\langle \mathbf{B}\cdot\delta(\boldsymbol{\nabla} B_x)\rangle \qquad (2)$$

This leads the DC and fluctuating magnetic fields and gradients to be kept below certain values in order to ensure proper science operation of the GW observatory. Due to the important role that magnetic effects play in eLISA, a set of magnetic sensors are required with the purpose of quantitatively identify the magnetic contribution that couples to the magnetic properties of the test mass and disturbs its motion. To that end, magnetometers aimed at reconstructing an accurate map of magnetic field and gradient in the region occupied by the TM.

The point of the magnetic sensing in eLISA has obviously been addressed first in its technology demonstrator called LISA Pathfinder. As a consequence, the selection criteria to identify the applicable magnetometer technology is performed in view of the previous experience with LISA Pathfinder, in which the selected typology was a set of four tri-axial fluxgate magnetometer. This technology was chosen on grounds of their long heritage in space applications and the ample sensitivity along the LISA Pathfinder measurement bandwidth ($1\,\mathrm{mHz} \leq \omega/2\pi \leq 30\,\mathrm{mHz}$). Looking towards eLISA, a number of further disadvantages were identified [4], which point to the study of alternative technologies to fluxgate magnetometers. Consequently, the main sensor characteristics that need to be addressed are: (i) compact sensor so as to allow more of them to be incorporated in the spacecraft, and moreover, improves the spatial resolution; (ii) sufficiently low magnetic and thermal back-action effects on the spacecraft environment to avoid disturbances, so that it can be placed closer to the TM [5]; (iii) low noise performance down to 0.1 mHz.

For the lower end of the eLISA bandwidth, magnetic field fluctuations across the TM are expected to be dominated by a time-varying interplanetary magnetic field not lower than $100\,\mathrm{nT\,Hz^{-1/2}}$ [6, 7], while the spacecraft's magnetic sources are expected to be the main contributor to the magnetic field gradient fluctuations [8]. Therefore, although eLISA requirements at subsystem level and the distribution of the magnetic sources in the spacecraft are still not formally defined, to be on the safe side, the noise performance of the the magnetic measurement system should be at least one order of magnitude less noisy than the expected interplanetary magnetic noise to be measured. It implies a sensitivity in the measurement system of

$$S^{1/2}_{B,\mathrm{system}} \leq 10\,\mathrm{nT\,Hz^{-1/2}},\ \omega/2\pi = 0.1\,\mathrm{mHz}. \qquad (3)$$

The work presented here has been also proposed as part of the magnetic field monitoring system within the STE-QUEST mission [9], a high-precision experiment of the weak equivalence principle using space atom interferometry. At the same way than in eLISA, some specific effects related to the lack of homogeneity of the magnetic field in the spacecraft can directly affect to the main scientific measurement of the mission. Hence, the stray magnetic field have to be suppressed below a certain level compatible with the targeted measurement accuracy. With the purpose of achieving the environmental magnetic conditions, a four-layer μ-metal shielding encloses the atom interferometer. In addition to passive shielding, the baseline design of STE-QUEST also foresees active magnetic compensation of slowly varying external fields (< 0.1 Hz). To this end, tiny magnetic sensors and compensation coils wound around the shield help to attenuate the slow external magnetic drifts within a continuous closed-loop mode. The size of the magnetometer is determined by the air gap between the subsequent shield layers (13 mm in the baseline design).

The motivation of using anisotropic magnetoresistive sensors (AMR) as an alternative to the conventional space qualified fluxgate magnetometer is increasing fast due to the mass, size and power restrictions for space applications [10, 11]. However, an important disadvantage of the AMR technology is the intrinsic $1/f$ noise that limits its use for applications requiring long integration time. A recent work has shown a noise level of $\sim 100\,\mathrm{nT\,Hz^{-1/2}}$ at 1 mHz [12], which clearly exceeds the value in Eq. (3). Besides, the noise performance of the sensor and its electronics has not been yet explored in the lower end of the eLISA bandwidth (0.1 mHz). For these reasons, in this paper we study the low-frequency noise behavior of a prototype based on magnetoresistive sensors with the dedicated noise reduction techniques, which are necessary to achieve the magnetic noise level requirements for eLISA[2]. The paper is organized as follows. In Sec. 2 a brief overview of the noise reduction techniques is explained. In Sec. 3 we analyze the noise and thermal contributions of the sensor and signal conditioning circuits to the overall noise. The experimental

[2]For a more demanding scenario, a parallel study was carried out using atomic magnetometer [13].

results are presented in Sec. 4, and finally, the main conclusions are drawn in Sec. 5.

2. Noise reduction techniques: Flipping and Electro-magnetic feedback

As considered further on the text, the intrinsic noise characteristics specified by the manufacturer of the magnetoresistors [14] are non-compliant with the low-frequency requirements for eLISA. For this reason, different electronic noise reduction techniques need to be assessed in order to minimize the sensor noise level in the eLISA frequency band. This section describes the methods to be studied.

2.1. Flipping

AMR sensors contain a thin film composed of a nickel-iron alloy with magnetic anisotropy. They have a sensitive axis to the magnetic field, and another axis aligned with the sensor magnetization called the *easy* axis. Taking advantage of these properties, flipping technique entails the periodic flip of the internal magnetization of the sensor strips by applying a switching field pulses (*set*/*reset* pulses) generated by a thin film conductor, which is wounded around the active area of the sensor [15]. The change of the magnetization direction induces the reversion of the output characteristic, as a result, the sensor output signal is modulated at the frequency of the switched pulses. Then, magnetic field measurements between each *set* and *reset* pulses are taken and subsequently demodulated. This sequence allows to subtract the bridge offset, since the offset voltage remains unchanged while the sensor output reverses the polarity. Fig. 1 shows the opposite slopes after the *set* and *reset* pulses, and the following offset voltage extraction for different bridge voltages. In addition, the main advantage of performing modulation techniques by using flipping pulses is the reduction of the $1/f$ noise within the desired bandwidth. One other advantage is the recovery of the output signal degradation induced from strong external magnetic fields ($> 300\,\mu$T), resolving an important drawback of magnetometers that use ferromagnetic core, such as fluxgates.

2.2. Electro-magnetic feedback

In order to minimize the coupling between temperature and magnetic field reading, the thermal dependence needs to be actively compensated during operation. Since the temperature drifts of the sensor sensitivity shows up as a gain error in the measurement, a feedback controller is devote to maintain the bridge

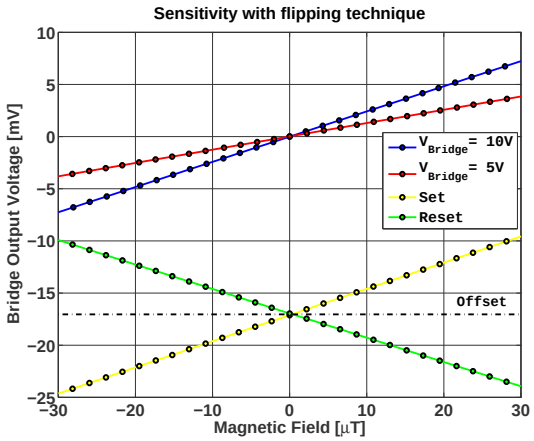

Figure 1: Output characteristics as a function of the magnetic field after a *set* (yellow trace) and *reset* (green trace) pulse with $V_{\text{bridge}} = 10\,\text{V}$. Bridge offset extraction is carried out for $V_{\text{bridge}} = 10\,\text{V}$ (blue trace) and $V_{\text{bridge}} = 5\,\text{V}$ (red trace).

output close to zero, which means in balanced bridge condition, so as to reduce the thermal effects. By using electro-magnetic feedback technique, an integrated coil involved in such closed-loop controller induces an opposing field to counteract the field component detectable by the sensor, then the current flowing through the compensation coil together the current-to-field conversion of the coil gives the strength of the magnetic field measurement. This method is particularly useful at the low frequencies where temperature drifts become more significant in the overall sensor noise.

3. Front-End Electronics

The analog signal conditioning for the magnetic field sensing with the flipping method is shown in Fig. 2. The Wheatstone bridge is made up of four magnetoresistors [14], whose output signal is amplified, low pass filtered, sampled and digitally demodulated.

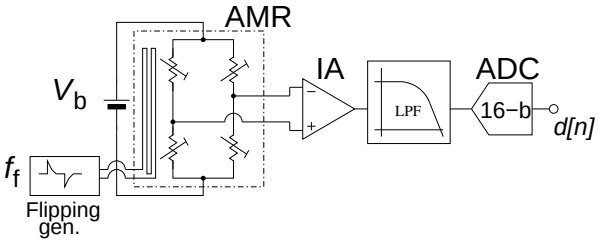

Figure 2: Analog signal processing scheme for flipping method.

The flipping generator circuit performs short *set*/*reset* pulses ($\tau \simeq 1\,\mu$s) with peaks of 3.3 A along a strap of

1.5 Ω. Although the circuit delivers high current peaks, the duration of the pulses is so short that the energy stemmed from the charged-up capacitor is very small ($E = 0.5\,C\,V^2 = 2.75\,\mu$J for $C = 0.22\,\mu$F). The flipping frequency f_f has been set to 5.5 Hz, enough to reduce the $1/f$ noise of the instrumentation amplifier (IA) by modulating the signal from the magnetometer. The selected modulation frequency is a trade-off among the $1/f$ noise reduction, the effects on the magnetic and thermal disturbances produced by a more periodic switching signal, and the transient response after the pulses. Magnetic field measurements are acquired 10 ms after each *set* and *reset* pulses, so that all the flipping currents have died down below micro-ampere level, and the low-pass filter settling time has elapsed. Therefore, glitches and transients in the immediate times after the flipping pulses are not seen by the analog-to-digital conversion process.

The analog signal conditioning for electro-magnetic feedback together with the flipping method is shown in Fig. 3. The electro-magnetic feedback circuit is a closed-loop controller, in which a current regulator feeds the compensation coil with the measured magnetic field. In order to force the sensor output signal to zero, which is the remaining error, an integrator is required in the control loop. The measured field strength is represented as voltage, proportional to the compensation current.

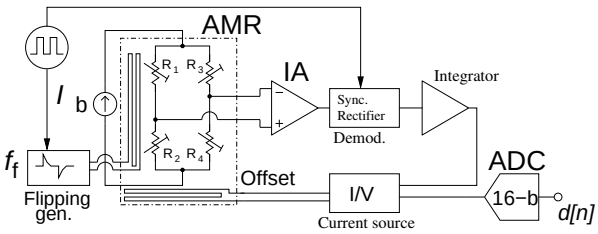

Figure 3: Analog signal processing scheme for electro-magnetic feedback and flipping.

3.1. Low-frequency noise analysis

The noise of the system can be split into two different parts. One coming from the intrinsic $1/f$ noise presented in the magnetometer itself, and the other one coming from the signal conditioning circuit. In the following we describe the main noise sources in the whole system.

The first stage of the circuit is the magnetic sensors constituted by a magnetoresistive Wheatstone bridge configuration. The nominal value of the resistors is $R_{b,n} = 850\,\Omega$ and the bridge output sensitivity is $s_b = s_{AMR} V_b = 136\,\mu$V μT^{-1}, where $s_{AMR} = 32\,\mu$V V^{-1} μT^{-1} is the AMR sensitivity and $V_b = 4.25$ V is the bridge voltage. Hence, the white-noise floor caused by the Johnson noise of the bridge resistances is $S^{1/2}_{AMR,\,T} = (4k_B T R_{b,n})^{1/2} = 3.75$ nV Hz$^{-1/2}$ at 300 K, where k_B is the Boltzmann constant. The voltage noise from the sensor is converted to equivalent magnetic field noise referred to the input dividing by the bridge sensitivity $S^{1/2}_{AMR,\,T}/(s_{AMR} V_b) = 27.6$ pT Hz$^{-1/2}$. From this equation and assuming additive noise, the higher the sensor sensitivity or the bridge voltage the lower the equivalent magnetic field noise. At low frequencies, the corner frequency of the $1/f$ noise is around 60 Hz, which leads to a sensor noise level of 21 nT Hz$^{-1/2}$ at 0.1 mHz. So, only the low-frequency contribution from the AMR is sufficient to exceed the requirements given in Eq. 3. Apart from the intrinsic $1/f$ behavior, the contribution due to the thermal drifts will deteriorate the noise performance. For these reasons, the electronic noise reduction techniques shown in Fig. 3 were implemented to overcome the noise limitations of the AMRs at the eLISA bandwidth.

The contribution of the bridge's source is negligible compared with the sensor noise. Besides, *ratiometric measurements* are performed in order to reduce drifts, noise or interference in the analog-to-digital conversion process. Hence, the voltage reference of the ADC is also employed to drive the bridge. The bridge output is amplified by a space-qualified low-noise IA (AD524) with a gain of 100 V V^{-1}. The output noise introduced by this stage considering the closed-loop transfer function can be modeled as [16]:

$$e^2_{o,\,IA}(f) = \left[e^2_{n,\,IA}\left(1 + \frac{f_{c,\,e_n}}{f}\right) + i^2_{n,\,IA}\left(1 + \frac{f_{c,\,i_n}}{f}\right) R_b^2 \right] \times \left| \frac{K_{eq} \cdot H_{int}}{1 + H_{oc} + K_{eq} \cdot K_{coil} \cdot H_{int}} \right|^2 , \quad (4)$$

where $e_{n,\,IA} = 7$ nV Hz$^{-1/2}$, $i_{n,\,IA} = 350$ fA Hz$^{-1/2}$, $f_{c,\,e_n} = 3$ Hz and $f_{c,\,i_n} = 30$ Hz are the input voltage/current spectral densities and their respective corner frequencies describing the noise characteristic of the IA, K_{eq} is the product of the IA gain and the bridge sensitivity s_b, K_{coil} is the gain of the voltage-to-current converter (4 mA/V) multiplied by the compensation coil ratio (1.96 μT/mA), and H_{int} and H_{oc} are the integrator and offset compensation responses. The signal from the magnetometer, i.e., the input signal to the amplifier, is modulated by applying flipping pulses. As a result, the noise level of the IA is the one at the frequency of the modulating signal. For the IA AD524 the equivalent

magnetic field noise with a modulating signal of only 5.5 Hz is 64 pT Hz$^{-1/2}$, consequently, fully compliant with the system requirements.

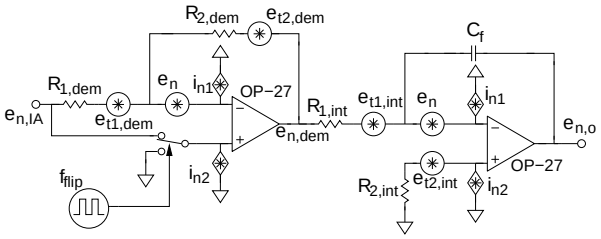

Figure 4: Demodulator and integrator circuit with the main contributions considered for the noise estimation.

The phase sensitive detector is synchronized with the flipping pluses using an analog switch, which alternates the sign of the unity gain amplifier in order to rectify the modulated signal. The noise contribution for both configuration (inverting and non-inverting amplifier) are not critical in the overall noise of the signal conditioning circuit. After the rectifier circuit the signal is demodulated and integrated. The output noise for the integrator is given by

$$e^2_{\mathrm{o,Int}} = \left[(e^2_{\mathrm{n}} + i^2_{\mathrm{n}}R^2_{2,\mathrm{int}} + e^2_{\mathrm{t2,int}})\left[1 + \left(\frac{f_{\mathrm{i}}}{f}\right)^2\right] + e^2_{\mathrm{t1,int}}\left(\frac{f_{\mathrm{i}}}{f}\right)^2 + i^2_{\mathrm{n}}R^2_{1,\mathrm{int}}\left(\frac{f_{\mathrm{i}}}{f}\right)^2\right] \times \left|\frac{1 + H_{\mathrm{oc}}(f)}{1 + H_{\mathrm{oc}}(f) + K_{\mathrm{eq}} \cdot K_{\mathrm{coil}} \cdot H_{\mathrm{int}}(f)}\right|^2 \quad (5)$$

where $f_{\mathrm{i}} = 1/(2\pi R_{1,\mathrm{int}}C_{\mathrm{f}})$, $e_{\mathrm{t1,int}}$ and $e_{\mathrm{t2,int}}$ is the thermal noise voltage of the resistor $R_{1,\mathrm{int}}$ and $R_{2,\mathrm{int}}$ (both of 10 kΩ), $e^2_{\mathrm{n}} = e^2_{\mathrm{nf}}(1 + f_{\mathrm{ce}}/f)$ and $i^2_{\mathrm{n}} = i^2_{\mathrm{nf}}(1 + f_{\mathrm{ci}}/f)$ are the amplifier input noise in terms of power voltage and power current density. The noise parameters of the op-amp are the noise floor ($e_{\mathrm{nf}} = 3\,\mathrm{nV\,Hz^{-1/2}}$ and $i_{\mathrm{nf}} = 0.4\,\mathrm{pA\,Hz^{-1/2}}$) and the corner frequency ($f_{\mathrm{ce}} = 2.7$ Hz and $f_{\mathrm{ci}} = 140$ Hz). Hence, the equivalent output noise of the integrator is around 51 pT Hz$^{-1/2}$ at 0.1 mHz.

Another integrator, named offset compensation, is also used between the output and the reference terminal of the AD524 in order to extract the offset of the modulated signal. The noise contribution of this circuit is not critical along the measurement bandwidth since the signal is still modulated at this stage.

The last stages in the closed-loop circuit is the current source to drive the compensation coil and the analog-to-digital converter (ADC) to measure the output voltage, which is proportional to the measured magnetic field. A *floating load* topology has been implemented on grounds of its simplicity and low-noise performance. Assuming a typical compensation coil ratio of 0.51 mA/μT, the estimated equivalent magnetic field noise applied by the current source has a noise floor around 4 pT Hz$^{-1/2}$. This value is negligible compared with the intrinsic noise of the sensor itself. Regarding the ADC (ADS7809), the manufacturer gives a maximum rms noise of 1.3 LSB (least significant bit). This leads to a spectral noise density of $1.3q/\sqrt{f_{\mathrm{s}}/2} = 1.4\,\mu\mathrm{V\,Hz^{-1/2}}$ (11 pT Hz$^{-1/2}$), where q is the ADC voltage resolution for a 16-bit ADC with a full scale range of 10 V (±5 V). This contribution dominates over the ADC quantification noise $q/\sqrt{12fs} = 0.2\,\mu\mathrm{V\,Hz^{-1/2}}$ (< 2 pT Hz$^{-1/2}$). Since the low-frequency noise characteristics of the ADC are not given by the manufacturer, the corner frequency of the $1/f$ noise has been found at 10 mHz by an experimental fit to the data.

Fig. 5 shows the theoretical output spectral noise density for the different stages of the signal conditioning circuit. As expected, the most important contribution at sub-millihertz frequencies is clearly the intrinsic $1/f$ noise of the AMR sensor, which is foreseen to be minimized in the experimental results by the flipping technique. We remark that although the $1/f$ noise of the sensor can be reduced, it can not be eliminated and is envisaged to continue being the dominant source in the overall noise of the system. In particular the resistors in the bridge still suffer at long times from a $1/f$ behavior and the *ac* excitation of the bridge does not totally eliminate it. Therefore, *excess* noise caused by current flows across the magnetoresistance bridge could be a significant contribution, which also exhibits a $1/f$ noise power spectrum [17, 18]. On the other hand, the electronic noise sources from the signal conditioning circuits are well bellow the magnetic requirement along the measurement bandwidth. This allows to unveil the noise improvement of the sensor itself when utilizing the different noise reduction techniques. The IA, ADC, and Johnson noise of the magnetoresistances can limit the noise performance at frequencies higher than 1 Hz, and thus outside the eLISA bandwidth.

3.2. Temperature coefficient analysis

The optimization of the thermal dependences in the sensors and the signal conditioning circuit is critical, since low-frequency temperature drifts may show up as an excess noise at sub-millihertz frequencies. One of the more sensitive elements to thermal changes are the resistors forming the Wheatstone bridge. Assuming the

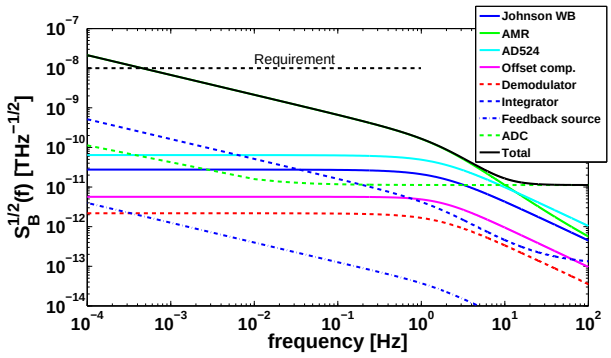

Figure 5: Theoretical equivalent magnetic field output noise of the signal conditioning circuit using flipping technique together with electro-magnetic feedback. Noise contribution of the AMR (green solid trace) shows the intrinsic noise of the sensor without flipping excitation. Its noise reduction due to the modulation technique is estimated experimentally in Sec. 4.

worst-case condition, the temperature coefficient (TC) of the bridge output voltage is

$$\alpha_\mathrm{b} \simeq 2V_\mathrm{b}\left[\frac{R_1R_2}{(R_1+R_2)^2}+\frac{R_3R_4}{(R_3+R_4)^2}\right]\cdot\alpha_\mathrm{R,AMR} \quad (6)$$

$$= V_\mathrm{b}\left(1-\frac{\Delta R_\mathrm{b}^2}{R^2}\right)\cdot\alpha_\mathrm{R,AMR} \simeq V_\mathrm{b}\cdot\alpha_\mathrm{R,AMR}, \quad (7)$$

where $\alpha_\mathrm{R,AMR} = 0.25\,\%\,\mathrm{K}^{-1}$ is the TC of the AMR. The bridge resistances $R_\mathrm{b,n}$ change by an amount $\Delta R_\mathrm{B} = s_\mathrm{AMR}R_\mathrm{b,n}B = \pm 1.088\,\Omega$ for a sensor range of $\pm 40\,\mu$T. $R_1 = R_4 = R_\mathrm{b,n} - \Delta R_\mathrm{b}$ and $R_2 = R_3 = R_\mathrm{b,n} + \Delta R_\mathrm{b}$ are the magnetoresistive components shown in Fig. 3. Therefore, the maximum TC of the Wheatstone bridge is $10.6\,\mathrm{mV\,K}^{-1}$ and the equivalent magnetic field noise can be calculated by

$$S^{1/2}_{B,\,\mathrm{WB}}(\omega) = \frac{\alpha_\mathrm{b}}{s_{\mathrm{b},\,\mathrm{AMR}}\cdot V_\mathrm{b}}\cdot S^{1/2}_{T,\,\mathrm{AMR}}(\omega), \quad (8)$$

where $S^{1/2}_{T,\,\mathrm{AMR}}$ is the thermal fluctuations in the magnetometer location. The thermal environment is not yet determined for eLISA, but the temperature fluctuations inside the satellite are expected to be lower than that one for LPF ($S^{1/2}_{T,\,\mathrm{LPF}} < 0.1\,\mathrm{K\,Hz}^{-1/2}$). This leads to an equivalent magnetic field noise referred to the input of $7.8\,\mu\mathrm{T\,Hz}^{-1/2}$, which is much larger than the requirement defined in Eq. 3. In view of the demanding stability and of the high thermal coefficient of the AMR [21], flipping and electro-magnetic feedback are also used with the purpose of reducing the thermal drift effects in the sensors.

With the flipping technique each magnetic readout is the average difference between two consecutive measurements with opposite polarization. Thus, the effect due to the temperature changes is now given by

$$\alpha_\mathrm{b} \simeq V_\mathrm{b}\frac{\Delta R_\mathrm{b}}{R_\mathrm{b,n}}\alpha_\mathrm{R,AMR}, \quad (9)$$

where α_b assuming the worst-case condition and a full unbalanced Wheatstone bridge (full-scale range) is reduced to $13.6\,\mu\mathrm{V\,K}^{-1}$ ($0.1\,\mu\mathrm{T\,K}^{-1}$). Then, the equivalent magnetic field fluctuations given by Eq. 8 is $10\,\mathrm{nT\,Hz}^{-1/2}$, which barely achieves the requirements.

When a constant voltage source feeds the bridge, the temperature dependency of the bridge resistance will vary the bridge output as $V_\mathrm{o} = V_\mathrm{b}\Delta R_\mathrm{b}/(R_\mathrm{b}(1+\alpha_\mathrm{R,AMR}T))$ for a worst-case error. In contrast, the temperature sensitivity can be improved using a constant current source instead, since variations in the resistances are partly compensated with changes in the voltage across the bridge. Then, the sensor output is equivalent to the constant current $V_\mathrm{o} = I_\mathrm{b}\Delta R_\mathrm{b}$ and the thermal stability is improved. Nevertheless, the AMR sensitivity also changes with temperature due to the energy-band structure of the magnetic material [22]. The error due to the temperature dependence of the sensor sensitivity is then $I_\mathrm{b}\alpha_\mathrm{sens}\Delta R_\mathrm{b} = 3.3\,\mu\mathrm{V\,K}^{-1}$ ($24\,\mathrm{nT\,K}^{-1}$) for a full-scale range of $\pm 40\,\mu$T. As can be seen in Fig.6, thermal dependences of the AMR bridge, more precisely the TC of the resistance and sensor sensitivity, are among the largest thermal contributions in the signal conditioning circuit and play a main role in the excess noise at low frequencies. As gain errors, they increase with ΔR_b, this is, as the Wheatstone bridge gets more unbalanced. As explained before, this effect is reduced using a negative closed-loop that follows a null ΔR_b to keep the bridge balanced, and therefore, the gain errors barely affect the measurement. The TCs for the different stages of the circuit are compared in Table 1, where thermal drifts of the operational amplifier parameters (bias current, offset current, and offset voltage) can be neglected.

4. Results: Low-frequency magnetic noise spectral density

4.1. Low-frequency noise: stray field measurements

Low-frequency noise measurements for characterizing the system were carried out by placing the device inside a three-layer μ-metal shielding. A bias field inside the shielding was not applied for these runs, therefore, a low residual field around $\sim 20\,\mathrm{nT}$ was measured

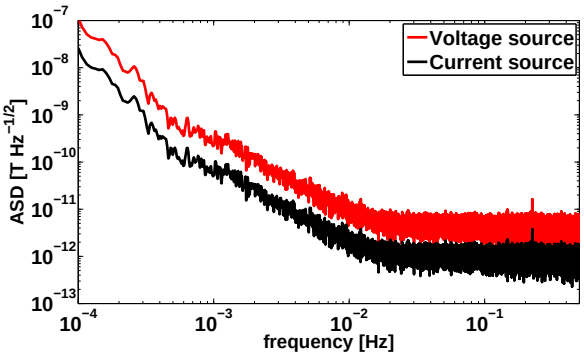

Figure 6: Equivalent field noise contribution due to thermal fluctuations in the laboratory and with full-scale field range. Thermal contributions were estimated for bridge's voltage (red) and current source (black).

Table 1: Temperature coefficients referred to the input for the stages of the electronics in which flipping and electro-magnetic feedback techniques were used. $I_b \Delta R_b$ is the bridge output voltage.

source	$TC_{rti} = k_{TC} \Delta R_b$ [V/K]	k_{TC}
WB resistor (Volt. source)	$\alpha_{R,AMR} V_b / R_b \Delta R_b$	1.3×10^{-5}
WB sensitivity	$\alpha_{sens} I_b \Delta R_b$	3.0×10^{-6}
Bias source	$\alpha_R I_b \Delta R_b$	3.0×10^{-9}
IA Gain drift	$\alpha_{GIA} I_b \Delta R_b$	1.2×10^{-7}
IA Offset compensation	$(\alpha^2_{R,oc} + \alpha^2_{C,oc})^{1/2} I_b \Delta R_b$	4.2×10^{-6}
Demodulator	$\alpha_{R,dem} I_b \Delta R_b$	3.0×10^{-9}
Integrator	$(\alpha^2_{R1,int} + \alpha^2_{Cf,int})^{1/2} I_b \Delta R_b$	4.2×10^{-6}
Compensation source	$\alpha_{R,cs} I_b \Delta R_b$	3.0×10^{-9}
ADC	$\alpha_{ADC} I_b \Delta R_b$	3.5×10^{-8}
$\text{Total}_{V-Source}$	$\sqrt{\Sigma TC^2_{rti}}$	1.5×10^{-5}
$\text{Total}_{I-Source}$		6.7×10^{-6}

by the sensor. Lock-in and flipping noise reduction techniques at different modulation frequencies (5.5 Hz and 10 Hz) were performed by using a voltage (5 V and 10 V) and a current source (5 mA) to supply the sensor. Fig. 7 shows the equivalent magnetic field spectral density measured by the system. Noise curves exhibit that ac excitation using lock-in amplification does not avoid the potential $1/f$ noise of the magnetoresistors, however, the flipping scheme helps to reduce part of it across the desired bandwidth. This contribution can not be totally mitigated and the noise measurements still exhibit a dominant $1/f$ behavior coming from the bridge's resistors. Owing to the TC reduction of the sensor, additional improvement in the millihertz bandwidth has been obtained when a low noise current source supplies the bridge instead of a voltage source [21], with a similar low-frequency noise to the fluxgate used in LISA Pathfinder. At higher frequencies, the noise level is slightly reduced at the expense of increasing flipping frequency and bridge voltage. In this case, additional disturbances in the spacecraft environment are caused because of the magnetic field created by the more periodic set/reset pulses and the self-heating effects coming from the dissipated power in the sensor. Since our interest is focused in the fluctuations in the low-frequency region, which is the limiting noise factor, flipping pulses at 5.5 Hz and a current bridge of 5 mA ($V_b = 4.25$ V) are the selected features.

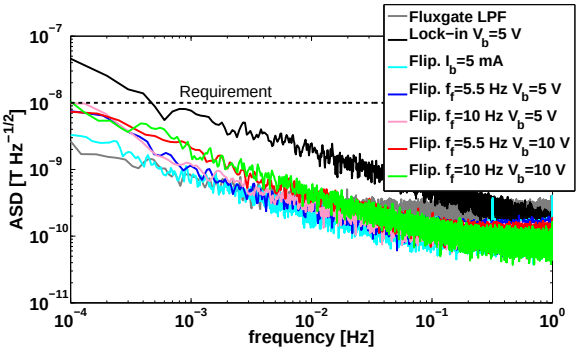

Figure 7: Equivalent magnetic field noise density for the engineering model of the fluxgate magnetometer used in LISA Pathfinder and an AMR sensor using lock-in amplification and flipping techniques. Measurements have been done driving the AMR sensor with voltage (V_b) and current source (I_b, cyan trace). Bias field is not applied.

4.2. Low-frequency noise under a bias magnetic field

Additional noise in the low frequency band appears as a consequence of the thermal dependence of the sensor coupled to the slow environmental temperature drifts. As shown in Table 1 the TC of the system depends on the amount of unbalance of the Wheatstone bridge, i.e., the magnitude of the magnetic field seen by the sensor. For noise investigation, a leading field of $\sim 21\,\mu$T with a stability better than 1 nT Hz$^{-1/2}$ at 0.1 mHz is applied by a coil inside the magnetic shielding. The purpose is to unbalance the bridge to stress the effect of the gain temperature coefficient of the sensor and conditioning circuit during the noise measurements.

Fig. 8 shows the noise measurements using the flipping technique and electro-magnetic feedback in the presence of a bias field. To begin with, we measured the stability of the current source that generates the

bias field and found it suitable to carry out the experiment. On the one hand for flipping method, the equivalent magnetic field noise at 0.1 mHz increases by an order of magnitude with respect to the previous results in Fig. 7 without leading field. As expected, the excess noise due to the thermal dependence is still more significant when a constant voltage source supplies the bridge. On the other hand, the noise curve for electro-magnetic feedback shows that the the effect of the gain temperature coefficient of the sensor is mitigated by the use of a proper closed-loop mode. The noise level achieved is $\sim 3\,\mathrm{nT\,Hz^{-1/2}}$ at 0.1 mHz, which is below the LPF requirement in Eq. (3) shifted to the eLISA frequency band. Therefore, this compensation method is determining to maintain long-term stability over temperature, and produces desirable results for measuring magnetic fields at the LISA frequencies. At higher frequencies, the noise floor is down to $\simeq 100\,\mathrm{pT\,Hz^{-1/2}}$ with the corner frequency at $\simeq 0.2$ Hz ($I_\mathrm{b} = 5$ mA and $f_\mathrm{f} = 5.5$ Hz), which might be reduced up to the Johnson noise of the bridge resistance by increasing the flipping frequency.

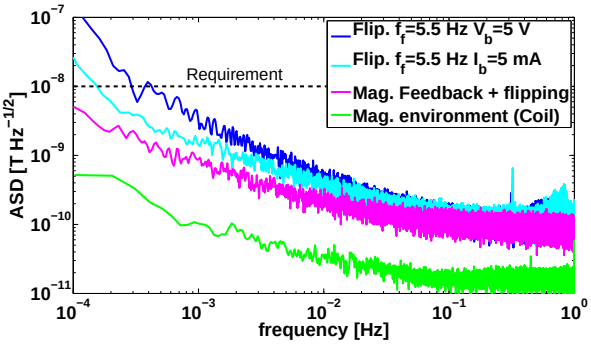

Figure 8: Spectral density in terms of equivalent magnetic field using flipping with voltage and current sources and electro-magnetic feedback. The green trace shows magnetic field noise generated by the coil at 15 mm from the sensor. The magnetic noise requirement at 0.1mHz (dashed trace) is achieved using electro-magnetic feedback (magenta trace). Bias field is $\sim 21\,\mu$T.

5. Conclusions

We have presented the low-frequency noise characterization of a magnetic field measuring system based on AMRs. Chip-scale magnetoresistive sensors appear as a solution to the disadvantages met with the bulky fluxgate magnetometers used in LISA Pathfinder. Nevertheless, magnetoresistors exhibit higher intrinsic noise characteristics than fluxgate magnetometers. Thus, in order to enhance the noise performance various methods have been analyzed and tested in the millihertz band. First, flipping techniques help to overcome part of the potential $1/f$ noise, which cannot be avoided with conventional lock-in amplification techniques. Secondly, an excess noise below 1 mHz is exhibited when magnetic field is applied to the sensor as a result of the temperature dependence of the system. A solution is found using electro-magnetic feedback in the signal conditioning circuit. A closed-loop controller with a compensation coil helps to overcome the thermal dependence and to minimize the additional noise in the bandwidth of interest. With the combination of these methods, the equivalent magnetic noise spectral density is well within the LPF requirement shifted down to the eLISA frequencies (0.1 mHz – 1 Hz). From the achieved low-frequency noise performance, AMR sensors with dedicated noise reduction techniques are presented as an alternative to the fluxgate sensors used in LISA Pathfinder. The technology points to be useful beyond the scope of eLISA, specially for space applications with strict restrictions in size, weight, and long-term stability.

Acknowledgments

We wish to thank Paleomagnetic group in the Earth Sciences Institute (CSIC/UB) for the availability of their facilities. Support for this work came from Project AYA2010-15709 of Plan Nacional del Espacio of the Spanish Ministry of Science and Innovation (MICINN).

[1] The eLISA Consortium, preprint (arXiv:1305.5720) (2013).
[2] F. Antonucci *et al*, Class. & Quantum Grav., **28**, 094002 (2011).
[3] P. Canizares *et al*, Class. & Quantum Grav., **26**, 094005 (2009).
[4] M. Diaz-Aguiló, E. García-Berro and A. Lobo, Class. & Quantum Grav., **27**, 035005 (2010).
[5] I. Mateos *et al.*, ASP Conf. Ser. **467**, 341 (2013).
[6] B. L. Schumaker, Class. & Quantum Grav., **20**, S239 (2003).
[7] A. Balogh *et al.*, Astron. Astrophys. Suppl, **92**, 221-236 (1992).
[8] M. Hueller, Class. & Quantum Grav., **22**, S521 (2005).
[9] T. Schuldt *et al*, Exp. Astron, **31**, 0922-6435 (2015).
[10] M. Díaz-Michelena, P. Cobos, C. Aroca, Sens. Actuators A, **222**, 149-159 (2015).
[11] P. Brown *et al*, Rev. Sci. Instrum., **23**, 059501 (2012).
[12] P. Brown *et al*, Rev. Sci. Instrum., **85**, 125117 (2014).
[13] I. Mateos *et al.*, Sens. Actuators A, **224**, 147-155 (2015).
[14] Honeywell, *1- and 2-axis magnetic sensors HMC1001, 1002, 1021, 1022*, 900248 Rev C (2008).
[15] H. Hauser, P. L. Fulmek, P. Haumer, M. Vopalensky, and P. Ripka, Sens. Actuators A, **106**, 121-125 (2003).
[16] R. Pallás and J. G. Webster, *Analog Signal Processing*, (John Wiley & Sons, New York, 2001).
[17] C.D. Motchenbacher and J.A. Connelly, *Low-noise electronic system design*, (John Wiley & Sons, 1993).
[18] F. N. Hooge, IEEE Trans. Electron Devices, **41** 11 (1994).
[19] H. Hauser, G. Stangl, W. Fallmann, R. Chabicovsky and K. Riedling, Proc. Workshop Preparation, Properties, and Applications of Thin Ferromagnetic Films (Viena), 15-27 (2000).

[20] I. Mateos *et al*, J. Phys.: Conf. Series, **154** 012005 (2009).
[21] I. Mateos *et al*, J. Phys.: Conf. Series, **363** 012051 (2012).
[22] C. Wu and A. chen, Phys. Rev. B, **18** 4 (1978).